Carbon 205 (2023) 27–32

Contents lists available at ScienceDirect

Carbon

journal homepage: www.elsevier.com/locate/carbon

Growth of high-density horizontal SWNT arrays by pre-cracking of carbon source

Tianze Tong [a], Weiming Liu [a], Jie Yan [b], Mingzhi Zou [a], Liu Qian [a,**], Jin Zhang [a,*]

[a] Center for Nanochemistry, Beijing Science and Engineering Center for Nanocarbons, Beijing National Laboratory for Molecular Sciences, College of Chemistry and Molecular Engineering, Peking University, Beijing, 100871, PR China
[b] College of Chemistry and Molecular Engineering, Peking University, Beijing, 100871, PR China

ARTICLE INFO

Keywords:
Single-walled carbon nanotubes
Horizontal arrays
High density
Cracking of carbon source

ABSTRACT

Obtaining high-density horizontal single-walled carbon nanotube (SWNT) arrays is the key point of developing SWNT-based integrated circuits. However, some catalysts showing good control over SWNT structures possess relatively low activity to grow SWNT, which restricts the density of the grown arrays. Therefore, we developed a rational method to grow high-density SWNT arrays by iron (Fe)-assisted pre-cracking of carbon source in gas phase. A tiny amount of Fe, decomposed from ferrocene, was introduced into the chemical vapor deposition system with the gas flow without forming Fe nanoparticles on the substrates. The density of the SWNT arrays grown from Mo_2C, WC and Cu catalysts can be significantly increased by 3–5 times with the help of Fe, reaching 40, 35 and 24 tubes μm^{-1}, respectively. Through gas chromatography and Raman spectrum characterization, it is proved that carbon source decomposed more completely with Fe in the gas phase, which resulted in higher utilization efficiency of carbon source and better quality of the grown SWNTs. This pre-cracking approach is an effective way to improve the density of SWNT arrays with controlled structures.

1. Introduction

Single-walled carbon nanotubes (SWNTs) exhibit outstanding electrical properties because of their nanoscale sizes and special structures, which is regarded as one of the most promising materials to manufacture next-generation carbon-based integrated circuits [1,2] (ICs). However, high-density SWNT arrays with uniform structures is necessary to realize the high performance and good device-to-device homogeneity of SWNT-based ICs [3], which is still a challenge in SWNT synthesis. Traditional methods to obtain high-density SWNT arrays mainly include post-treatment methods and direct growth methods. Although SWNT arrays with very high density can be obtained through post-treatment methods, such as gold-film-assisted transfer [4] and the classic Langmuir-Blodgett method [5], their purity and alignment are both poor due to polymer impurities and carbon nanotube bundles formed during the treatment process, resulting in undesirable performance reduction of the SWNT-based devices. Directly growing SWNT arrays by chemical vapor deposition (CVD) can usually obtain samples with better alignment, less defects and damage, compared with the approaches mentioned before. Typical methods include patterning catalysts stripe [6], multiple loading catalysts [7], multi-cycle growth [8], reactivation of catalysts [9] and Trojan catalyst methods [10]. However, catalysts used in these methods were commonly metal nanoparticles with high catalytic activities, leading to the growth of high-density SWNT arrays without structural control. Therefore, improving the growth efficiency of those catalysts which show good control over SWNT structures is an effective way to achieve good structural uniformity and high-density at the same time.

Based on the understanding of SWNT growth mechanism [11,12], there are two important periods in the growth of SWNTs: the decomposition of carbon source with catalysts at high temperature and the assembly of SWNTs on the catalysts. Therefore, the growth efficiency of the SWNT is partly determined by the decomposition efficiency of carbon source (η) and the rate of the carbon fragments assembling into SWNTs (ν), which greatly influence the obtained density (D) of the SWNT arrays. It can be described as:

$$D \propto \eta \times \nu.$$

Ethanol is a commonly used carbon source in CVD growth of SWNTs.

* Corresponding author.
** Corresponding author.
E-mail addresses: qianliu-cnc@pku.edu.cn (L. Qian), jinzhang@pku.edu.cn (J. Zhang).

https://doi.org/10.1016/j.carbon.2022.12.086
Received 30 November 2022; Received in revised form 28 December 2022; Accepted 30 December 2022
Available online 3 January 2023

However, for many kinds of catalysts, their ability of decomposing ethanol is limited, especially for some carbide catalysts [13,14], which have been used to synthesize SWNTs with controlled structures [15]. The relatively low η is the key stumbling block restricting the density of SWNT arrays grown from these catalysts on substrates. Apart from this, the low η of these catalysts lead to the incompletely decomposition of ethanol, resulting in the formation of amorphous carbon [16], which heavily decreases the active lifetime of catalysts and the quality of SWNTs.

Herein, we developed a rational approach to improve the SWNT growth efficiency by introducing Fe to assist the carbon source decomposition process in gas phase. A tiny amount of Fe, decomposed from ferrocene, was introduced into CVD system with gas flow. With the help of Fe, the activation energy for ethanol to decompose decreases, increasing the concentration of high-activity carbon species near the catalyst. As a result, the density of the SWNT arrays grown from Mo_2C, WC and Cu catalysts can be significantly increased by 3–5 times, reaching 40, 35 and 24 tubes μm^{-1}, respectively. And a highest density of 80 tubes μm^{-1} was obtained through this strategy. This pre-cracking method with the help of gas phase Fe is a promising approach to obtain high-density SWNT arrays with controlled structures in the future.

2. Material and methods

2.1. Synthesis of horizontal SWNT arrays on sapphire substrates

In our experiments, the a-plane sapphire substrates (single-side polished, miscut angle $<0.5^o$, surface roughness <5 Å) purchased from Hefei Kejing Materials Technology Co., China were used as substrates for growing SWNT. Before the growth process, the sapphire substrates were cleaned and annealed at 1100 °C in air for 8h for better crystallization. The catalyst precursor solution ($(NH_4)_6Mo_7O_{24}\bullet 4H_2O$, $(NH_4)6W_7O_{24}\bullet 6H_2O$, $Cu(NO_3)_2$ 0.05 mmol/L, 15 μL) was spin coated onto the substrate and the substrate was then placed at the center of a tube furnace in a 1-inch quartz tube (850 °C). After an oxidation process in air, the tube was purged with 300 sccm argon (Ar) for 5 min. H_2 (0–300 sccm) was then introduced into the tube for 5 min, followed by the introduction of carbon source (ethanol, which can release O species during the reaction to etch the amorphous carbon, lengthening the lifetime and alleviating the poisoning of catalysts to get a higher growth efficiency) for catalyst carbonization and SWNT growth. After growth for 15 min, the furnace was cooled to room temperature in an argon and hydrogen atmosphere. For Fe-assisted growth process, the Fe was introduced into the tube by Ar gas (50–100 sccm) flowing through the ethanol solution of ferrocene (0.5 μmol/L).

2.2. Characterization of Fe content in reaction exhaust by inductive coupled plasma emission mass Spectrometer (ICP-MS)

The sample was collected by pumping the reaction exhaust of the Fe-assisted growing system into a gas scrubber, and the content of Fe was detected by ICP-MS with high detection sensitivity after long time enrichment to prove that Fe indeed existed in gas phase by argon bubbling into the reaction system. The specific collection process is as follows: The tail pipe of the system was connected to a gas scrubber containing 300 mL HNO_3 solution (6.5%). Before collecting the gas, the reaction tube was purged by argon gas, then the argon flow was adjusted to 200 sccm through the ethanol solution of ferrocene, and the gas flow was maintained for 12 h. The collection of exhaust and the characterization of Fe content was conducted multiple times at different time points during the ventilation process, in order to obtain the relationship between the total amount of Fe carried into the CVD system and time. During the bubbling process, the Fe element carried into the exhaust gas was captured by HNO_3 and stayed in the solution phase. Then the solution after bubbling was diluted four times before ICP-MS detection.

2.3. General characterization

X-ray photoelectron spectroscopy (XPS) were analyzed by AXIS Supra X-ray Photoelectron Spectrometer (Kratos Analytical Ltd.) with Al Kα (1486.6 eV) as the X-ray source. Scanning electron microscope (SEM) images were collected by Hitachi S4800 under 1.0 kV and 10 kV. Raman spectra were obtained on Jovin Yvon-Horiba LabRam systems with excitation laser: 532 nm. Atomic force microscope (AFM) images were obtained by Dimension Icon microscope (Bruker). Gas chromatography-Mass Spectrometer (GC-MS) tests were carried out using Shimadzu GCMS-TQ8050.

2.4. Calculations of ethanol decomposition process with and without introduction of Fe

DFT calculations were performed with the Vienna ab-initio simulation package (VASP) code (version 5.4.4) [17]. The Revised Perdew-Burke-Ernzenhof from Hammer et al. (RPBE) functional [18] within the generalized gradient approximation (GGA) regime was used to describe the electron exchange-correlation interaction. The core-valence electrons interactions were modeled with the projector augmented wave (PAW) method [19,20]. The Kohn-Sham equations were solved in a plane wave basis set with a kinetic energy cutoff of 400 eV. The convergence criteria for the electronic self-consistent iteration and force were set to be 10-6 eV and 0.03 eV/ Å, respectively. The first Brillouin zone was sampled with a Γ-centered $1 \times 1 \times 1$ Monkhorst-Pack k-point mesh. Transition states were located using the climbing image nudged elastic band (CI-NEB) method [21,22]. The convergence criteria for the electronic self-consistent iteration and force were set to be 10-6 eV and 0.05 eV/ Å, respectively.

3. Results and discussion

A group of controlled experiments with or without the introduction of gas phase Fe were performed, as shown in Fig. 1a. Ferrocene ($FeCp_2$) was used as Fe precursor because it can easily evaporate and decompose into Fe at high temperature. In order to limit the content of Fe in the gas phase to avoid the nanoparticle deposition on the substrate, an ultra-low concentration (0.5 μmol/L) of ferrocene was dissolved in ethanol and introduced into the system with Argon gas flowing through. We first used WC as catalyst to grow SWNTs. As expected, once added Fe into the system, the density of the horizontal SWNT array increased from 6 tubes μm^{-1} to 35 tubes μm^{-1}, up by 5 times approximately. The SEM images of the arrays are shown in Fig. 1b and c. And the large-view SEM images at low magnification in Fig. S1 also show the homogeneity of the high-density SWNT arrays in large scale. With the introduction of Fe, a highest density of 80 tubes μm^{-1} can be obtained from the AFM image inset Fig. 1c. This is the highest density that have been reported using WC as catalyst, indicating that Fe help to facilitate a more efficient use of WC catalyst nanoparticles.

In order to verify the universality of this approach, we used Mo_2C, another carbide as the catalyst to grow SWNT arrays. As illustrated in Fig. 2a–c, SEM and AFM were used to characterize the density of SWNT arrays. The results show that the density of SWNT arrays grown from Mo_2C catalyst increased almost 3 times, from 12 tubes μm^{-1} to 40 tubes μm^{-1} with the introduction of Fe. On top of that, we also used copper (Cu), a metal catalyst with relatively low activity, to grow SWNTs, and the results are shown in Fig. 2d–f. The density of the grown SWNT arrays increased from 8 tubes μm^{-1} to 24 tubes μm^{-1}, up by 2 times approximately. Metal catalysts and carbide catalysts are two kinds of representative catalysts in the field of SWNT growth by CVD method. These results indicated that introducing Fe in gas phase is an effective strategy to improve the growth efficiency of SWNTs on other catalysts, thus increasing the density of the SWNT array. Besides, ST-cut quartz was also used as the substrate to load Cu catalysts and synthesize SWNT

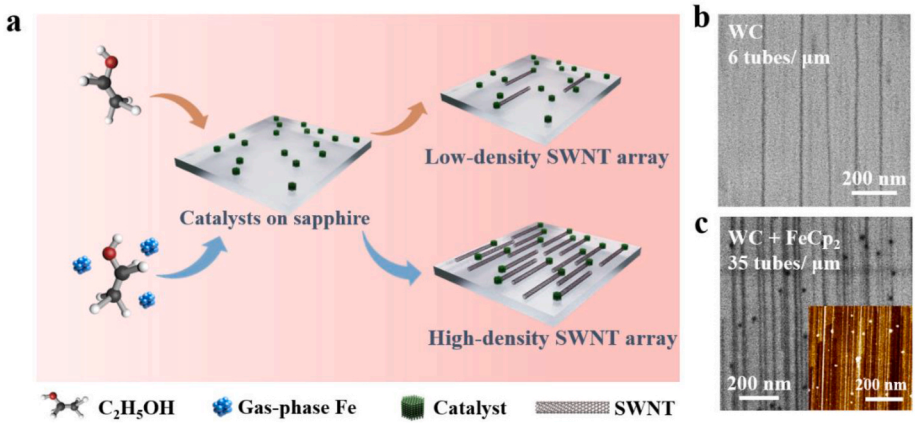

Fig. 1. The schematic of Fe-assisted pre-cracking of carbon source strategy to grow high density horizontal SWNT arrays. (a) The sketch map of controlled experiments which using Fe-assisted pre-cracking of carbon source strategy or not. (b) The SEM image of the SWNT array grown from WC without the introduction of Fe. (c) The SEM and AFM (inset) images of the SWNT array grown from WC with the introduction of Fe. (A colour version of this figure can be viewed online.)

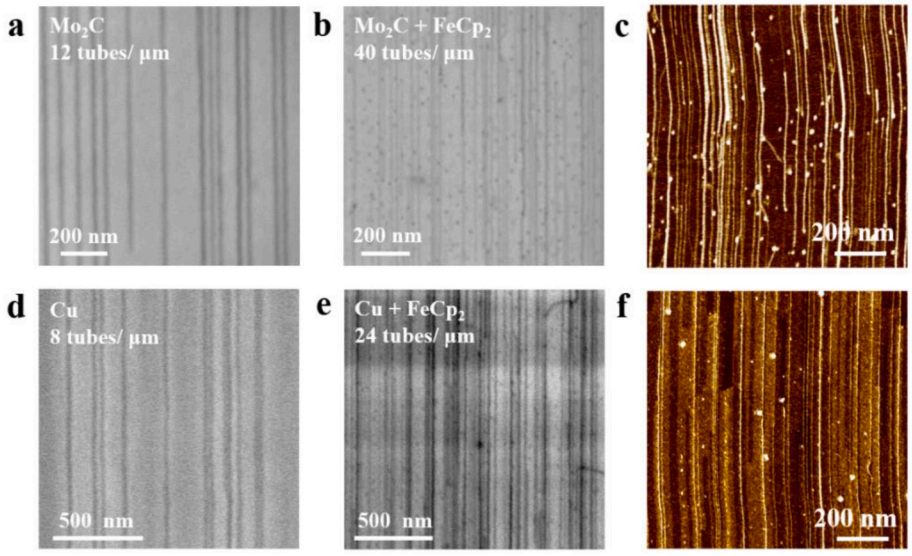

Fig. 2. The universality of Fe-assisted pre-cracking strategy to grow high density horizontal SWNT arrays. (a) The SEM image of the SWNT array grown from Mo_2C without the introduction of Fe. (b–c) The SEM (b) and AFM images (c) of SWNT arrays grown from Mo_2C with the introduction of Fe. (d) The SEM images of SWNT arrays grown from Cu without the introduction of Fe. (e–f) The SEM (e) and AFM images (f) of SWNT arrays grown from Cu with the introduction of Fe. (A colour version of this figure can be viewed online.)

arrays. The density of the grown SWNT arrays almost doubled after introducing Fe into the reaction system, as shown in Fig. S2, revealing the universality of this Fe-assisted strategy.

In order to figure out the role of Fe in the growth process, a series of characterizations were performed. Using WC as catalysts, the reaction exhaust from the CVD system with the introduction of Fe was collected and pumped into a gas scrubber with HNO_3 solution, and the content of Fe element was then detected by ICP-MS with high detection sensitivity. As illustrated in Fig. 3a, with the increase of collecting time, the concentration of Fe element increased linearly, and the coefficient of determination is 0.95. Obviously, Fe existed in gas phase, which indicates that using Ar flow bubbling through the ethanol solution of ferrocene is an effective way to bring Fe into the gas phase with a stable rate. Meanwhile, the content of Fe on sapphire substrate after growth was measured by XPS. As shown in Fig. 3b, no Fe signal was detected on the sapphire surface, indicating scarcely any Fe deposition on the substrate. Therefore, when blank sapphire without any catalyst deposition was used as a substrate in Fe-assisted growth system, no SWNTs were found on the substrate (inset of Fig. 3b), which means that Fe cannot form nanoparticles on the substrate to grow SWNTs. This result is consistent with the XPS result [23].

GC-MS was then used to analyze the decomposition of carbon source under different conditions, as shown in Fig. S3. Exhaust gas was collected during the growth process when using pure ethanol without catalysts, ethanol solution of $FeCp_2$ (0.5 μmol/L) without catalysts, pure ethanol with WC catalysts and ethanol solution of $FeCp_2$ (0.5 μmol/L) with WC catalysts. Through separating and analyzing the component of the exhaust gas, Fig. 3c and d extracted the relative content of C_2H_4 and CH_4 under the aforementioned four different conditions. The results show that introducing a small amount of Fe in gas phase led to much higher content of C_2H_4 and CH_4, and the using of WC catalysts on substrates also brought about the increase of C_2H_4 and CH_4, but lower than that with Fe only. It is worth noting that the content of Fe that introduced into the system was much less than WC, indicating a much higher ability of Fe to decompose ethanol. When WC catalysts and gas phase Fe were both introduced into the system, a highest decomposition efficiency can be expected, but the content of C_2H_4 and CH_4 is lower than using WC catalysts only. This result demonstrates that more high-activity carbon species were transferred into SWNTs. Raman spectroscopy was used to analyze the quality of the SWNTs on the substrates. As shown in Fig. 3e and f, the intensity ratio of G/D mode (I_G/I_D) is 14 using WC catalyst only, but increasing to 4531 with gas phase Fe. The contrast demonstrates reduced formation of amorphous carbon and better quality of SWNTs on the substrates when introducing Fe into the system, indicating that gas-phase Fe facilitates a highly effective transformation of carbon source to SWNTs [24]. The images for RBM modes of Raman

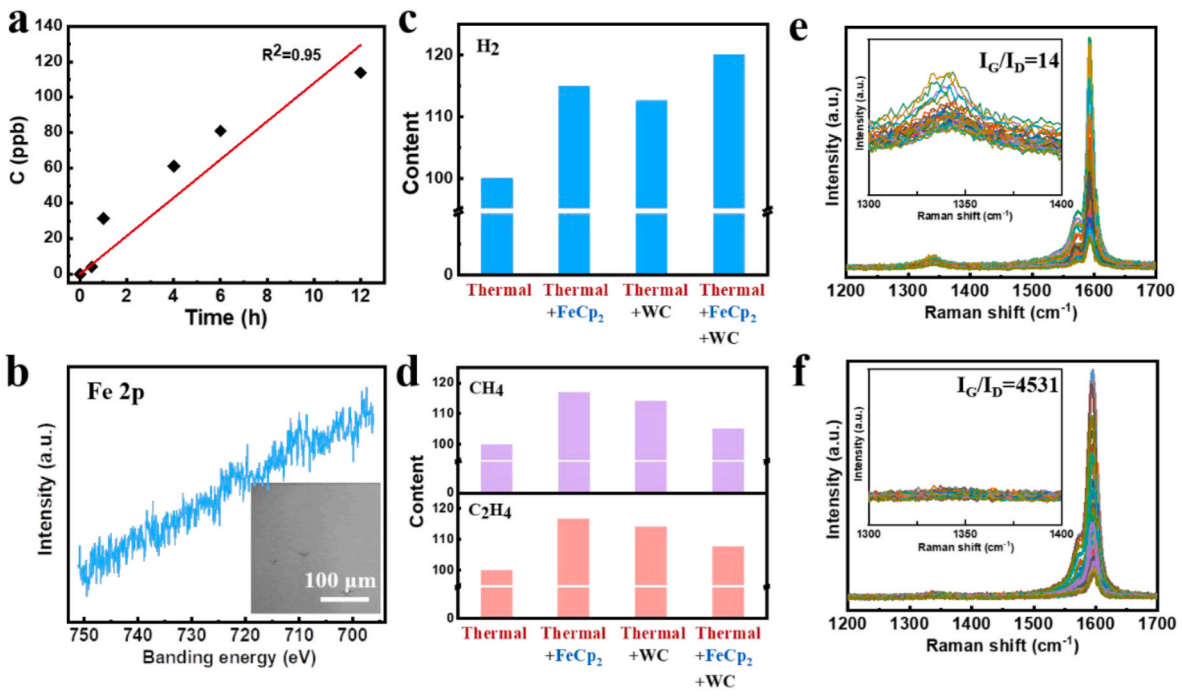

Fig. 3. The characterization of Fe-assisted pre-cracking strategy to grow high-density horizontal SWNT arrays. (a) The content of Fe in gas phase with the introduction time measured by ICP-MS. (b) XPS spectrum in Fe 2p region of the sapphire substrate surface after SWNT growth. Inset is the SEM image of a controlled experiment which introduced Fe without loading WC catalysts. (c–d) Relative content of C_2H_4 (c) and CH_4 (d) in reaction exhaust under different collecting conditions measured by GC-MS. (e–f) Raman line mapping spectra of SWNT arrays grown from WC without (e) and with (f) the introduction of Fe. (A colour version of this figure can be viewed online.)

spectra are demonstrated in Fig. S4.

From the above results it can be deduced that the gas-phase Fe mainly plays a role in the process of carbon-source decomposition. As shown in Fig. 4a, with Fe nanoclusters in gas phase, a more sufficient decomposition of ethanol can be speculated because of the higher catalytic activity of Fe, and the decomposed carbon species can be mostly used to grow SWNTs without forming amorphous carbon and wrapping the catalyst nanoparticle. On the contrary, a less sufficient decomposition of carbon source may cause the deposition of more amorphous carbon and poison the catalyst nanoparticle, resulting in lower growth efficiency of SWNTs. Therefore, the gas-phase Fe actually functions as a pre-cracking catalyst for carbon source, facilitating the SWNT growth on other catalysts. To further understand the mechanism of this pre-cracking methods, density functional theory (DFT) calculations of ethanol decomposition process were performed at 0 K to describe the reaction possibility. As shown in Fig. 4b and c, ethanol decomposed into C_2 dimer through a series of reactions, the energy barrier of each reaction decreased significantly with the participation of gas-phase Fe. Thus, according to Arrhenius equation, in reaction temperature, the reaction rate of EtOH catalytic decomposition with Fe-assisted pre-cracking is much faster than the thermal decomposition. On the basis, the presence of Fe in gas phase decided the decomposition degree of EtOH and the concentration of high activity carbon species in the reaction system, which determines the density of SWNT arrays.

The above calculation reveals that Fe contributes to the cracking of C–H bonds, so we can predict the effect of gas-phase Fe acting on different catalyst systems according to the catalysts' ability of cracking C–H bonds. Therefore, besides Mo_2C [13] and WC [14], another two metal catalysts, Fe [25] and Pd [26], with better ability of cracking C–H bonds were also used as catalysts to grow SWNTs. The growth results were shown in Fig. S5 and the ratios of densities with and without the introduction of Fe were illustrated in Fig. 4d, together with the activation energy of cracking C–H bonds for the four different catalysts [13,14,25,26]. When Fe was introduced, Mo_2C and WC grew SWNT arrays with higher densities. However, for Pd and Fe catalysts, the introduction of gas phase Fe decreased the density of SWNT arrays on the contrary. In EtOH molecular, the C–H bond has the highest bond energy and is the most difficult bond to be broken, the activation energy of C–H bond for different catalysts represents the ability of the catalyst to crack the carbon source. Therefore, it can be concluded that for catalysts showing relatively low ability to crack carbon sources, the introduction of gas-phase Fe can significantly increase the density of SWNT arrays. However, for catalysts with strong catalytic cracking ability, like Pd and Fe, the SWNT-array density decreases after the introduction of Fe, which may be due to the catalyst poisoning and deactivation caused by the deposition of excessively cracked carbon source.

4. Conclusion

In summary, we developed a Fe-assisted pre-cracking carbon source strategy to improve the activity of catalysts on substrates and grow high-density SWNT arrays. For catalysts with relatively low catalytic activity, with the help of Fe in gas phase, the carbon source can be decomposed more completely to supply more high-activity carbon species to catalysts on substrates, which decreases the deposition of amorphous carbon and increases the growth efficiency of SWNTs. Through this pre-cracking carbon source method, the density of SWNT arrays can be increased by 3–5 times. Specially, using WC as catalysts, the density of SWNTs array can be increased to a highest density of 80 tubes μm^{-1}. This work provides a new strategy to synthesize high-density horizontal SWNT arrays and can be used to improve the density of SWNT arrays with controlled structures, promoting the development of carbon nanotube based nanoelectronics.

CRediT authorship contribution statement

Tianze Tong: Conceptualization, Investigation, Visualization, Writing – original draft. **Weiming Liu:** Conceptualization,

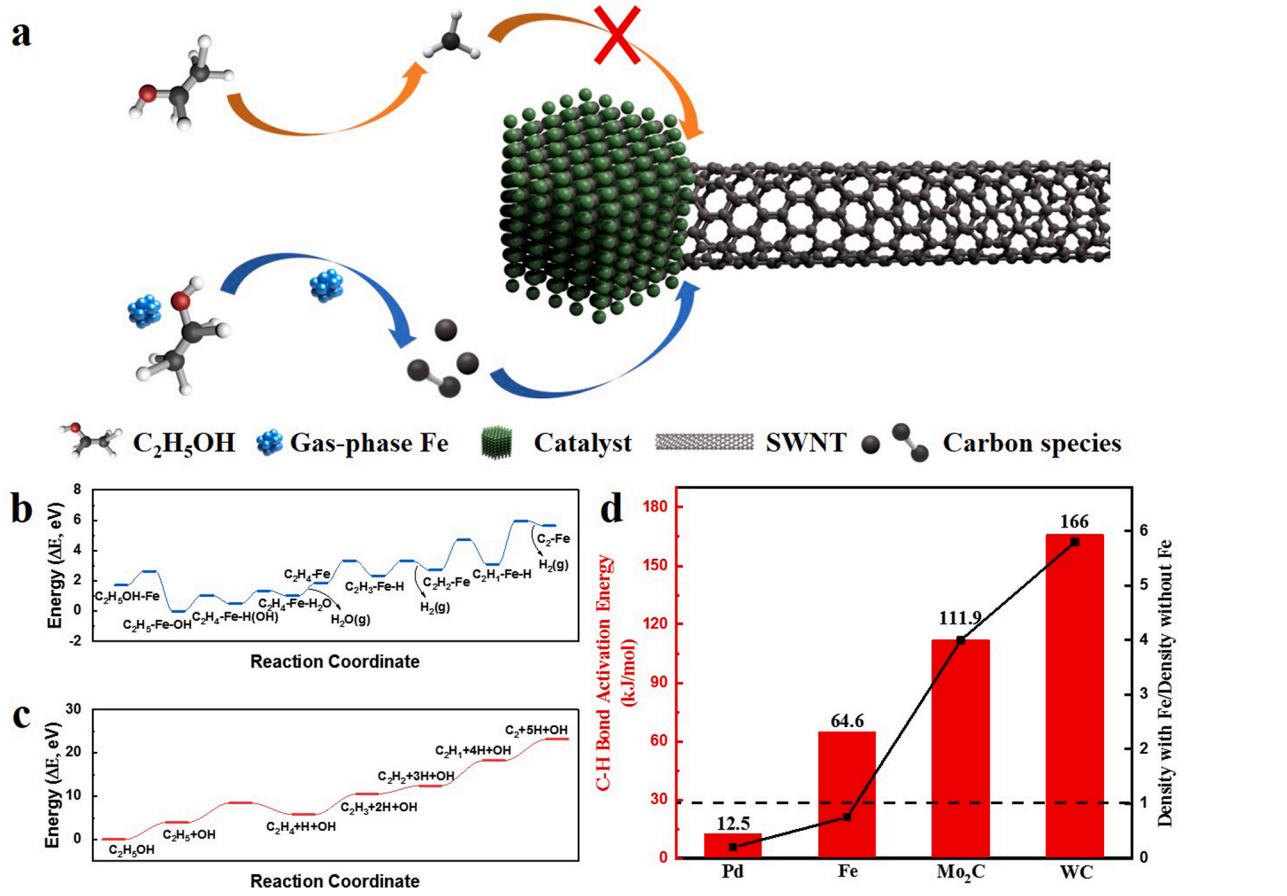

Fig. 4. (a) The illustration of carbon source utilization process in SWNT growth without or with the introduction of Fe. Calculated energy barriers of ethanol decomposition with (b) and without (c) gas-phase Fe. (d) The density increasing ratio of the SWNT arrays grown with and without gas phase Fe for different catalysts and their C–H bond activation energy [13,14,25,26]. (A colour version of this figure can be viewed online.)

Methodology, Validation. **Jie Yan:** Methodology, Validation. **Mingzhi Zou:** Visualization, Validation. **Liu Qian:** Conceptualization, Funding acquisition, Validation, Visualization, Writing – review & editing. **Jin Zhang:** Conceptualization, Funding acquisition, Project administration, Supervision, Validation, Writing – review & editing.

Declaration of competing interest

The authors declare that they have no known competing financial interests or personal relationships that could have appeared to influence the work reported in this paper.

Acknowledgement

This work was financially supported by the Ministry of Science and Technology of China (2016YFA0200100 and 2018YFA0703502), the National Natural Science Foundation of China (Grant Nos. 52021006, 51720105003, 21790052, 21974004, and 52102032), the Strategic Priority Research Program of CAS (XDB36030100), the Beijing National Laboratory for Molecular Sciences (BNLMS-CXTD-202001) and the Specific Program of China Postdoctoral Scientific Foundation (2022T150008).

Appendix A. Supplementary data

Supplementary data to this article can be found online at https://doi.org/10.1016/j.carbon.2022.12.086.

References

[1] G.S. Tulevski, A.D. Franklin, D. Frank, J.M. Lobez, Q. Cao, H. Park, et al., Toward high-performance digital logic technology with carbon nanotubes, ACS Nano 8 (9) (2014) 8730–8745.
[2] G. Hills, C. Lau, A. Wright, S. Fuller, M.D. Bishop, T. Srimani, et al., Modern microprocessor built from complementary carbon nanotube transistors, Nature 572 (7771) (2019) 595–602.
[3] A.D. Franklin, The road to carbon nanotube transistors, Nature 498 (7455) (2013) 443–444.
[4] M.M. Shulaker, H. Wei, N. Patil, J. Provine, H.-Y. Chen, H.S.P. Wong, et al., Linear increases in carbon nanotube density through multiple transfer technique, Nano Lett. 11 (5) (2011) 1881–1886.
[5] Q. Cao, S.-j. Han, G.S. Tulevski, Y. Zhu, D.D. Lu, W. Haensch, Arrays of single-walled carbon nanotubes with full surface coverage for high-performance electronics, Nat. Nanotechnol. 8 (3) (2013) 180–186.
[6] L. Ding, D. Yuan, J. Liu, Growth of high-density parallel arrays of long single-walled carbon nanotubes on quartz substrates, J. Am. Chem. Soc. 130 (16) (2008) 5428–5429.
[7] S.W. Hong, T. Banks, J.A. Rogers, Improved density in aligned arrays of single-walled carbon nanotubes by sequential chemical vapor deposition on quartz, Adv. Mater. 22 (16) (2010) 1826–1830.
[8] W. Zhou, L. Ding, S. Yang, J. Liu, Synthesis of high-density, large-diameter, and aligned single-walled carbon nanotubes by multiple-cycle growth methods, ACS Nano 5 (5) (2011) 3849–3857.
[9] Z. Wang, Q. Zhao, J. Zhang, Increasing the density of single-walled carbon nanotube Arrays by multiple catalysts reactivation, J. Phys. Chem. C 122 (43) (2018) 24823–24829.
[10] Y. Hu, L. Kang, Q. Zhao, H. Zhong, S. Zhang, L. Yang, et al., Growth of high-density horizontally aligned SWNT arrays using Trojan catalysts, Nat. Commun. 6 (1) (2015) 1–6.
[11] L.P. Ding, B. McLean, Z. Xu, X. Kong, D. Hedman, L. Qiu, et al., Why carbon nanotubes grow, J. Am. Chem. Soc. 144 (12) (2022) 5606–5613.
[12] A.J. Page, Y. Ohta, S. Irle, K. Morokuma, Mechanisms of single-walled carbon nanotube nucleation, growth, and healing determined using QM/MD methods, Acc. Chem. Res. 43 (10) (2010) 1375–1385.
[13] Y. Shi, Y. Yang, Y.-W. Li, H. Jiao, Activation mechanisms of H2, O2, H2O, CO2, CO, CH4 and C2Hx on metallic Mo2C (001) as well as Mo/C terminated Mo2C (101)

from density functional theory computations, Appl. Catal. A-Gen. 524 (2016) 223–236.
[14] T. Zhang, D. Holiharimanana, X. Yang, Q. Ge, DFT study of methane activation and coupling on the (0001) and (11-20) surfaces of α-WC, J. Phys. Chem. C 124 (49) (2020) 26722–26729.
[15] S. Zhang, L. Kang, X. Wang, L. Tong, L. Yang, Z. Wang, et al., Arrays of horizontal carbon nanotubes of controlled chirality grown using designed catalysts, Nature 543 (7644) (2017) 234–238.
[16] M. He, X. Duan, X. Wang, J. Zhang, Z. Liu, C. Robinson, Iron catalysts reactivation for efficient CVD growth of SWNT with base-growth mode on surface, J. Phys. Chem. B 108 (34) (2004) 12665–12668.
[17] G. Kresse, J. Furthmüller, Efficient iterative schemes for ab initio total-energy calculations using a plane-wave basis set, Phys. Rev. B 54 (16) (1996), 11169.
[18] B. Hammer, L.B. Hansen, J.K. Nørskov, Improved adsorption energetics within density-functional theory using revised Perdew-Burke-Ernzerhof functionals, Phys. Rev. B 59 (11) (1999) 7413.
[19] G. Kresse, D. Joubert, From ultrasoft pseudopotentials to the projector augmented-wave method, Phys. Rev. B 59 (3) (1999) 1758.
[20] P.E. Blöchl, Projector augmented-wave method, Phys. Rev. B 50 (24) (1994), 17953.
[21] G. Henkelman, B.P. Uberuaga, H. Jónsson, A climbing image nudged elastic band method for finding saddle points and minimum energy paths, J. Chem. Phys. 113 (22) (2000) 9901–9904.
[22] G. Henkelman, H. Jónsson, Improved tangent estimate in the nudged elastic band method for finding minimum energy paths and saddle points, J. Chem. Phys. 113 (22) (2000) 9978–9985.
[23] A. Grosvenor, B. Kobe, M. Biesinger, N. McIntyre, Investigation of multiplet splitting of Fe 2p XPS spectra and bonding in iron compounds, Surf. Interface Anal. 36 (12) (2004) 1564–1574.
[24] M.S. Dresselhaus, G. Dresselhaus, R. Saito, A. Jorio, Raman spectroscopy of carbon nanotubes, Phys. Rep. 409 (2) (2005) 47–99.
[25] J. Li, E. Croiset, L. Ricardez-Sandoval, Effects of metal elements in catalytic growth of carbon nanotubes/graphene: a first principles DFT study, Appl. Surf. Sci. 317 (2014) 923–928.
[26] V. Fung, F.F. Tao, D.-e. Jiang, Low-temperature activation of methane on doped single atoms: descriptor and prediction, Phys. Chem. Chem. Phys. 20 (35) (2018) 22909–22914.